

## Three-Dimensional Self-Collapse of Langmuir Waves

A. Y. Wong and P. Y. Cheung

*Department of Physics, University of California, Los Angeles, California 90024*

(Received 19 December 1983)

Experimental observation of Langmuir-wave collapse in three dimensions is presented with regard to collapse rate and threshold. Collapse proceeds under its own trapped field even after the decoupling from the external driver.

PACS numbers: 52.35.Mw, 52.35.Ra

Since the fundamental work by Zakharov<sup>1</sup> on Langmuir-wave collapse and strong turbulence, and the independent experimental discovery of cavitons,<sup>2</sup> there has been intense interest in this subject. Numerical calculations<sup>3,4</sup> and computer simulations<sup>5,6</sup> have demonstrated repeatedly the occurrence of self-collapse of Langmuir waves in two and three dimensions. By self-collapse, we mean the contraction of the Langmuir wave trapped inside the density cavity into small spatial dimensions under the influence of ponderomotive force. Once collapse is initiated, the process will continue even if the driver is terminated or decoupled. This is possible in three dimensions because the ponderomotive force resulting from the trapped field increases as  $L^{-3}$ , whereas the convective loss only increases as  $L^{-2}$ , where  $L$  is the size of the contracting wave field. Through the process of collapse, the plasma can reach a granular state<sup>7</sup> in physical and phase spaces composed of density cavities and localized fields. Experimental observation of collapse is important to the understanding of strong Langmuir turbulence in plasmas and to the confirmation of the self-collapse process in the presence of kinetic effects and electron nonlinearities which are not fully explored in analytical models.<sup>1</sup> Previous experimental measurements were obtained either in only one spatial dimension or in an inhomogeneous plasma.<sup>2,8-10</sup>

In this paper, we would like to present both spatial and temporal measurements in an unmagnetized, homogeneous plasma which quantitatively verify the theoretical description of the collapse process. This instability is excited in a beam-plasma system whose previous results<sup>9</sup> have demonstrated the existence of spiky turbulence and the simultaneous emission of harmonic radiation. A fast electron beam with parameters of  $k_0 a_0 \approx 6$ ,  $v_b/v_e \approx 30$ ,  $\Delta v_{\parallel}/v_b \leq 2\%$ , and  $n_b/n_0 \approx (0.4-2)\%$  ( $k_0$  is the initial wave number,  $a_0$  is the initial spatial half-width of the beam,  $v_b/v_e$  is the ratio of beam velocity to electron thermal velocity,  $\Delta v_{\parallel}$  is

the parallel beam spread, and  $n_b/n_0$  is the ratio of beam density to plasma density) is injected into a large, unmagnetized argon plasma with typical characteristics of  $n_0 \approx (2-3) \times 10^9 \text{ cm}^{-3}$ ,  $T_e \approx 1 \text{ eV}$ , and  $T_e/T_i \gg 1$ . A significant improvement over the previous experimental setup is a new, specially designed probe system which can make *in situ* measurements of various macroscopic quantities such as electric fields and density perturbations in two spatial dimensions (i.e., both along and transverse to the beam axis). As a result, the complete two-dimensional (2D) spatial and temporal evolutions of the electric field and density cavity during the collapse process are obtained. Since there is no observed asymmetry in the transverse plane, the 2D measurements are an actual representation of the 3D field and density patterns. Directional energy analyzers<sup>11</sup> with an angular resolution of  $\theta = \tan^{-1}(v_{\perp}/v_{\parallel}) \approx 3^\circ$  ( $v_{\parallel}$  and  $v_{\perp}$  are the parallel and perpendicular beam velocities, respectively) are used to measure the beam distribution and beam spatial profile. One of the analyzers can be rotated with respect to the beam axis to ensure that proper values of  $v_{\parallel}$  and  $v_{\perp}$  are obtained, and the complete distribution function of the beam,  $f_b(v_{\parallel}, v_{\perp}, t)$ , can be constructed. This is crucial in understanding the decoupling of the beam from the wave packet during the collapse process. The electric field and density cavity are sampled and time averaged at various times with use of a boxcar integrator to construct the temporal evolution of their spatial profiles. Single-shot data are also obtained with a fast storage oscilloscope.

The linear cold-beam instability quickly saturates because of beam-particle trapping.<sup>12,13</sup> The observed saturated electric field scales as a function of beam density, as predicted by the cold-beam relation  $E_0^2/W_b \propto (n_b/n_0)^{1/3}$ , where  $E_0^2$  is the wave intensity and  $W_b$  is the beam energy density. Using the experimental measured beam density of  $n_b/n_0 \approx 0.5\%$ , we estimate the normalized saturated wave intensity to be  $\bar{W}_0 = E_0^2/8\pi n_0 T_e \approx 0.3$

$\gg (k_0\lambda_D)^2 \gg m_e/m_i$ , where  $\lambda_D$  is the electron Debye length and  $m_e/m_i$  is the electron-to-ion mass ratio. The electric field is measured by wire probes which are calibrated by a diagnostic electron-beam probe in a smaller plasma device.<sup>10</sup> These measurements are compared with those obtained by measuring the amount of side scattering that the electric field imposes on the main electron beam during the experiment. Knowledge of the initial beam profile and the radial extent of the field makes this a relatively simple and reliable measurement, and the two sets of values are in good agreement with each other. The intensity of the beam-driven unstable wave exceeds the threshold of collapse [ $\bar{W}_0 > (k_0\lambda_D)^2$ ] and initiates the collapse process. The nonlinear development of this instability leads to a rapid localization of high-frequency plasma waves trapped inside collapsing density cavities.

For low beam densities,  $0.1\% \leq n_b/n_0 \leq 0.6\%$ , such as in this experiment ( $n_b/n_0 \approx 0.5\%$ ), a single localized peak is found at a well defined location away from the point of beam injection where the beam-driven wave reaches its maximum amplitude initially. The fact that the collapse process occurs at this location in a reproducible manner from shot to shot allows the use of repetitive sampling techniques to investigate the spatial and temporal behavior of the collapse process. Single-shot data, including magnetic-loop data on enhanced radiation emitted at the harmonic of plasma frequency,  $2\omega_p$ , are also used to monitor the collapse process. Figure 1 shows the time-averaged temporal evolution of the electric field at selected times during the collapse process. At  $\omega_{pi}t \approx 5.7$ , the initial field structure has an axial width (full width at half maximum) of  $\Delta z/\lambda_D \approx 500$  and a radial width of  $\Delta r/\lambda_D \approx 150$ . For  $\omega_{pi}t \leq 12$ , the spatial contraction is mainly along the beam direction. This is reasonable as the pumping beam sets a preferred direction for the initial development of the instability, which is essentially 1D. At  $\omega_{pi}t \approx 32.9$ , the field structure appears to be breaking up, and the spatial widths have contracted to  $\Delta z/\lambda_D \approx 160$  and  $\Delta r/\lambda_D \approx 93$ . As the electric field collapses, the point of maximum field intensity moves towards the beam source. At  $\omega_{pi}t \approx 55.8$ , the field has contracted both axially and transversely to  $\Delta z/\lambda_D \approx 42$  and  $\Delta r/\lambda_D \approx 39$ . Soon after this time,  $\Delta r$  stops contracting and remains approximately constant at  $\Delta r/\lambda_D \approx 43$ . Both the increase of the field intensity and the contraction of the axial width proceed at a much slower rate. When  $\omega_{pi}t \approx 78$ , the axial width is  $\Delta z/\lambda_D \approx 20$  and the field structure has an

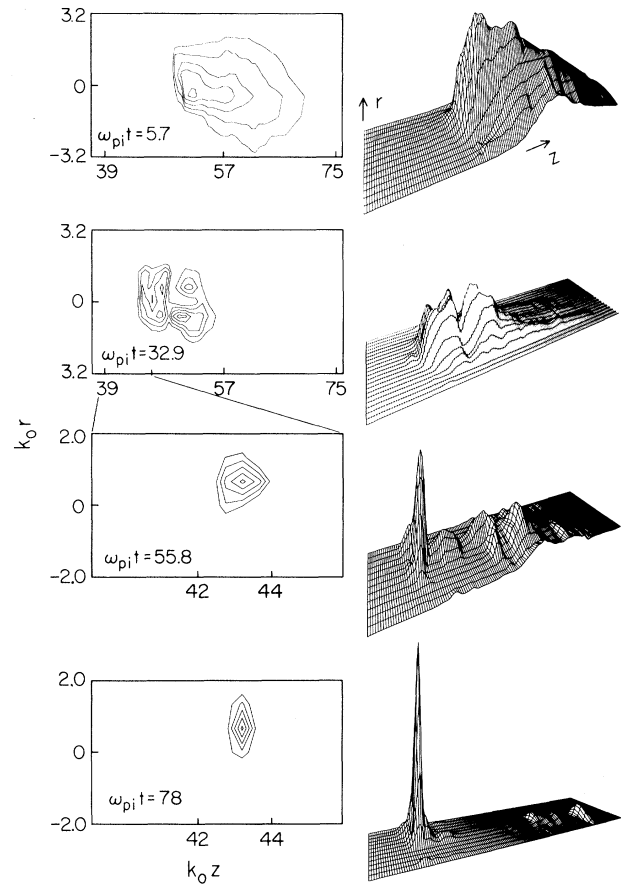


FIG. 1. Two-dimensional contours and three-dimensional views of wave intensity,  $E^2(r,z)$ , at  $\omega_{pi}t \approx 5.7, 32.9, 55.8,$  and  $78$ , respectively. The contours are in equal increments, with the value of the outermost contour at 0.35 of the peak wave intensity at each time. At  $\omega_{pi}t \approx 78$ , the peak intensity is approximately  $E^2/8\pi n_0 T_e \approx 1$ .

elongated, pancake shape with the ratio of transverse to axial width approximately equal to 2.

Theoretically, the time dependence of the collapse rate can be estimated with use of the Zakharov equations,<sup>1</sup> since our initial wave intensity is estimated to be  $E_0^2/8\pi n_0 T_e \approx 0.3 \gg (k_0\lambda_D)^2 \gg m_e/m_i$ , the wave packet is expected to collapse supersonically, and the Zakharov equations can be combined to give a contraction rate<sup>14</sup> of  $L \propto (t_0 - t)^{2/d}$ , where  $L$  is the width of the caviton field,  $d$  is the number of spatial dimensions, and  $t_0$  is defined as the time it takes the field to collapse to a singular point. For 3D Langmuir collapse,  $d=3$ , and the rate of contraction becomes  $L \propto (t_0 - t)^{2/3}$ .

The contraction rates of the spatial widths are plotted in Fig. 2. The vertical scales are in units of  $\Delta z/\lambda_D$  and  $(\Delta r/\lambda_D)^{3/2}$ , respectively. The radial

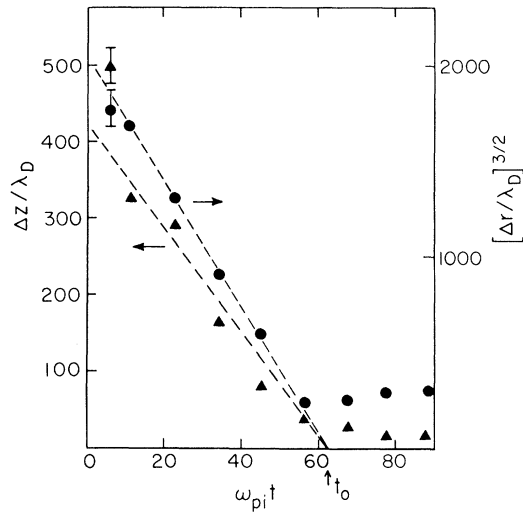


FIG. 2. Contraction rates of spatial widths of caviton. Axial widths (triangles) are in units of  $\Delta z/\lambda_D$  and the radial widths (circles) are in units of  $(\Delta r/\lambda_D)^{3/2}$ . Extrapolation of the contraction rates (dashed lines) determines  $t_0$ . Deviation from theory starts just before  $t_0$ .

contraction is observed to scale approximately as  $\Delta r/\lambda_D \propto t^{2/3}$  or  $(\Delta r/\lambda_D)^{3/2} \propto t$ , as shown in Fig. 2. The axial-width data points are more scattered and the contraction is roughly linear in time. By extrapolating the contraction rates before  $\omega_{pi}t < 58$ ,  $t_0$  is found to be at  $\omega_{pi}t \approx 62.5$ . After  $\omega_{pi}t > 58$ , the contraction in both directions is significantly slower and deviates from theory. At such small scale lengths, transit-time damping<sup>15</sup> and electron nonlinearities become important and must be taken into account. At higher beam densities,  $n_b/n_0 > 0.6\%$ , multiple collapsing wave packets are created along the beam path as was reported previously.<sup>9</sup>

Figures 3(a)–3(c) show the beam velocity distribution functions before and after the wave packet has collapsed. The beam is strongly scattered and its distribution function broadens before collapse occurs [Fig. 3(b)]. As the wave packet collapses, the beam-wave resonance is detuned as the effective wave number increases, and the beam begins to decouple from the wave. As a result, the beam propagates through the interaction region relatively unperturbed [Fig. 3(c)] and can excite new waves further downstream. This is in good qualitative agreement with theoretical predictions of beam decoupling<sup>16</sup> and nonlinear beam stabilization<sup>6</sup> during collapse.

A further proof of beam decoupling and self-collapse is demonstrated by shutting off the beam and monitoring the behavior of the electrostatic

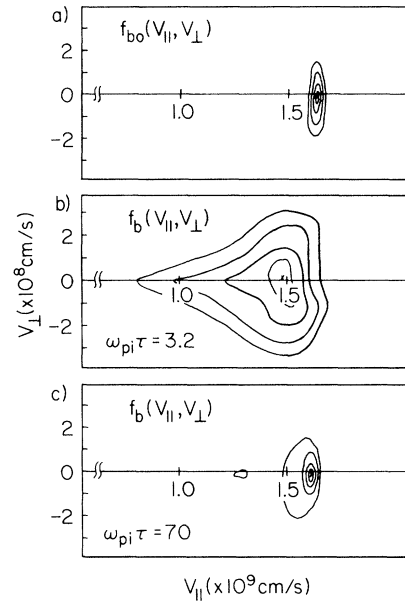


FIG. 3. Contours of electron beam distribution functions  $f_b(v_{||}, v_{\perp})$ : (a) initially with  $\Delta v_{||}/v_b \approx 1.6\%$  and  $\Delta v_{\perp}/v_b \approx 8.3\%$ ; (b) before collapse at  $\omega_{pi}t \approx 3.2$  with  $\Delta v_{||}/v_b \approx 26\%$  and  $\Delta v_{\perp}/v_b \approx 22\%$ ; and (c) after collapse at  $\omega_{pi}t \approx 70$  with  $\Delta v_{||}/v_b \approx 4.4\%$  and  $\Delta v_{\perp}/v_b \approx 10.2\%$ . The contours are in equal increments with the value of the outermost contour at 0.3 of  $f_b(v_{||}, v_{\perp})$ .

field of the collapsing caviton and its electromagnetic emission. Figure 4 shows single-shot data of this emission at twice the plasma frequency,  $2\omega_p$ . This harmonic emission is found to correlate with the collapsing caviton<sup>9</sup> and continues even after the beam is shut off. Although the wave packet contin-

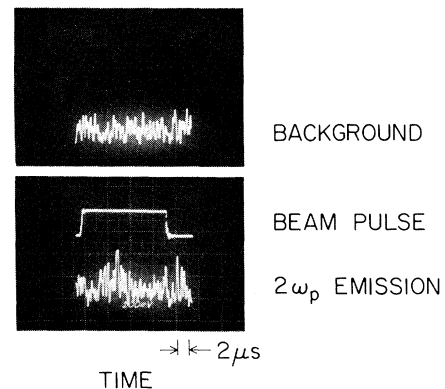


FIG. 4. Single-shot data of electromagnetic emission emitted at twice the plasma frequency,  $2\omega_p$ . The top trace is the noise background without the beam, the middle trace is the beam pulse, and the bottom trace is the  $2\omega_p$  emission received with a 3-MHz bandwidth detection system.

ues to collapse, it begins to move randomly after the beam is shut off. Its amplitude and location fluctuate from shot to shot and become extremely irreproducible. As a result, the temporal evolution of the spatial profile of the collapsing wave packet cannot be reconstructed by time averaging over many shots as is done when the beam is on.

In conclusion, we have observed experimentally the three-dimensional collapse process. The transverse contraction rate of the wave packet is observed to follow theoretical predictions until other nonlinear effects become important at small scale lengths. The relatively weak beam is observed to decouple from the wave packet and propagates relatively unperturbed through the interaction region.

This research was supported by the National Science Foundation under Grant No. PHY82-04363.

<sup>1</sup>V. E. Zakharov, *Zh. Eksp. Teor. Fiz.* **62**, 1745 (1972) [*Sov. Phys. JETP* **35**, 908 (1972)].

<sup>2</sup>H. C. Kim, R. L. Stenzel, and A. Y. Wong, *Phys. Rev. Lett.* **33**, 886 (1974).

<sup>3</sup>L. M. Degtyarev, V. E. Zakharov, and L. I. Rudakov, *Fiz. Plazmy* **2**, 438 (1976) [*Sov. J. Plasma Phys.* **2**, 240 (1977)]; N. R. Pereira, R. N. Sudan, and J. Denavit, *Phys. Fluids* **20**, 936 (1977).

<sup>4</sup>B. Hafizi, J. C. Weatherwell, M. V. Goldman, and D. R. Nicholson, *Phys. Fluids* **25**, 392 (1982); K. Nishi-

kawa, Y. C. Lee, and C. S. Liu, *Comments Plasma Phys.* **2**, 63 (1975).

<sup>5</sup>Yu. S. Sigov and V. E. Zakharov, *J. Phys. (Paris) C* **7**, 63 (1979); S. I. Anisimov, M. A. Berezovskii, M. F. Ivanov, I. V. Petrov, A. M. Rubenchick, and V. E. Zakharov, *Phys. Lett. A* **92**, 32 (1982).

<sup>6</sup>H. L. Rowland, J. G. Lyons, and K. Papadopoulos, *Phys. Rev. Lett.* **46**, 346 (1981); H. L. Rowland and K. Papadopoulos, *Phys. Rev. Lett.* **39**, 1276 (1977).

<sup>7</sup>A. S. Kingsep, L. I. Rudakov, and R. N. Sudan, *Phys. Rev. Lett.* **31**, 1482 (1973); A. Y. Wong, *Bull. Am. Phys. Soc.* **28**, 1213 (1983).

<sup>8</sup>A. Y. Wong and B. H. Quon, *Phys. Rev. Lett.* **34**, 1499 (1975).

<sup>9</sup>P. Y. Cheung, A. Y. Wong, C. B. Darrow, and S. J. Qian, *Phys. Rev. Lett.* **48**, 1348 (1982).

<sup>10</sup>P. Leung, M. Q. Tran, and A. Y. Wong, *Plasma Phys.* **24**, 567 (1982).

<sup>11</sup>R. L. Stenzel, W. Gekelman, N. Wild, J. M. Urruita, and D. Whelan, *Rev. Sci. Instrum.* **54**, 1302 (1983).

<sup>12</sup>W. E. Drummond, J. H. Malmberg, T. M. O'Neil, and J. R. Thompson, *Phys. Fluids* **13**, 2422 (1970).

<sup>13</sup>S. Kainer, J. Dawson, R. Shanny, and T. Coffey, *Phys. Fluids* **15**, 493 (1972); S. Kainer, J. Dawson, and T. Coffey, *Phys. Fluids* **15**, 2419 (1972).

<sup>14</sup>A. A. Galeev, R. Z. Sagdeev, V. D. Shapiro, and V. I. Shevchenko, *Zh. Eksp. Teor. Fiz.* **46**, 1352 (1977) [*Sov. Phys. JETP* **46**, 711 (1977)].

<sup>15</sup>A. Y. Wong, P. Leung, and D. Eggleston, *Phys. Rev. Lett.* **39**, 1407 (1977).

<sup>16</sup>A. A. Galeev, R. Z. Sagdeev, V. D. Shapiro, and V. I. Shevchenko, *Zh. Eksp. Teor. Fiz.* **45**, 507 (1977) [*Sov. Phys. JETP* **45**, 266 (1977)]; R. Z. Sagdeev, *Rev. Mod. Phys.* **51**, 1 (1979).

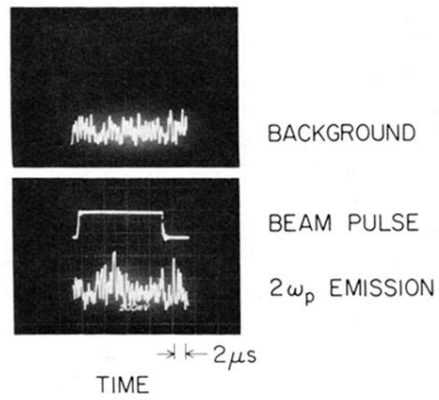


FIG. 4. Single-shot data of electromagnetic emission emitted at twice the plasma frequency,  $2\omega_p$ . The top trace is the noise background without the beam, the middle trace is the beam pulse, and the bottom trace is the  $2\omega_p$  emission received with a 3-MHz bandwidth detection system.